processes

MDPI

*Article*

# Shale Gas Productivity Prediction Model Considering Time-Dependent Fracture Conductivity

**Yuan Pan [1,2,3], Yiwen Xu [4], Ze Yang [1,2,3], Chunli Wang [5] and Ruiquan Liao [1,2,3,*]**

1 School of Petroleum Engineering, Yangtezu University, Wuhan 430100, China; panyuan_yangtzeu@163.com (Y.P.); yz942019@163.com (Z.Y.)
2 The Multiphase Flow Laboratory of Gas Lift Innovation Center, China National Petroleum Corporation, Wuhan 430100, China
3 Key Laboratory of Drilling and Production Engineering for Oil and Gas, Wuhan 430100, China
4 Engineering Institute of Engineering Technology, Xinjiang Oilfield Company, Karamay 834000, China; xywhold123@163.com
5 Research Institute of Exploration and Development, Petrochina Changqing Oilfield Company, Xi'an 710016, China; wcl2_cq@petrochina.com.cn
* Correspondence: 100619@yangtzeu.edu.cn; Tel.: +86-135-0721-2378

**Abstract:** Conventional shale gas productivity prediction techniques consider fracture conductivity to be a fixed value, but in actual production processes, conductivity changes with time. Therefore, this paper proposed a capacity prediction method that considers time-dependent conductivity and validates its accuracy using commercial simulators. First, relevant parameters were obtained by fitting the improved long-term conductivity test, and then the shale gas seepage model was established using the EDFM method. The laboratory test results showed that the order of significance affecting the conductivity retention rate was fracturing fluid viscosity > sand concentration > fracturing fluid retention time; the calculation results of the production prediction model show that the flow and the pressure curves that corresponded to constant conductivity and variable conductivity were to some extent different. In the presence of complex fractures and natural fractures, the increase in the variable conductivity production curve was smaller than that of the constant conductivity production curve. This study provides some guidance for field production.

**Keywords:** shale gas; fracturing horizontal wells; production prediction; time-dependent fracture conductivity

check for updates

**Citation:** Pan, Y.; Xu, Y.; Yang, Z.; Wang, C.; Liao, R. Shale Gas Productivity Prediction Model Considering Time-Dependent Fracture Conductivity. *Processes* **2022**, *10*, 801. https://doi.org/10.3390/pr10050801

Academic Editors: Tiankui Guo and Yidong Cai

Received: 23 March 2022
Accepted: 17 April 2022
Published: 19 April 2022

**Publisher's Note:** MDPI stays neutral with regard to jurisdictional claims in published maps and institutional affiliations.

**Copyright:** © 2022 by the authors. Licensee MDPI, Basel, Switzerland. This article is an open access article distributed under the terms and conditions of the Creative Commons Attribution (CC BY) license (https://creativecommons.org/licenses/by/4.0/).

## 1. Introduction

Shale gas is an important unconventional natural gas resource [1], and the multi-stage fracturing of horizontal wells is a key technology used to increase the level of production in the development of shale gas fields [2]. Due to the difference between shale reservoirs and conventional reservoirs [3], the question of how to accurately evaluate and predict the productivity of multi-stage fracturing wells remains a research hotspot. Traditional gas well dynamic analyses and productivity evaluations often focus on the influence of the physical properties of reservoirs, and they assign a certain value to fracture conductivity [4,5]. However, in the actual production process, the diversion capacity constantly changes with time, and its impact on the production capacity cannot be ignored.

There are many factors that affect the conductivity of hydraulic fractures, including the properties of the fracturing fluid [6], the proppant [7] itself, and its interaction with the reservoir rock [8]. As the production progresses, the proppant is broken and embedded [9], the fractures are gradually closed, and the conductivity is gradually reduced [10]. Studies have shown that proppant embedment is more severe when the rock is exposed to a water-softened state, potentially losing up to 88% of conductivity [11]. Obadare et al. proposed a fracture conductivity prediction model that considered dynamic data as they argued

that changes in conductivity are related to the degree of breakage within fracturing fluid gel [12]. Yu et al. studied the change law concerning the conductivity of propped fractures alongside the proppant loading concentration; the stress sensitivity of conductivity was weaker when the proppant loading concentration was higher [13]. Wang et al. believed that the placement form of a proppant had a great influence on conductivity [14].

The mainstream yield forecasting methods mainly include analytical methods (including semi-analytical methods), numerical simulation methods, and some machine learning methods [15–17]. The models of analytical methods are too simplified, and they do not have high calculation accuracy. The machine learning methods are similar to the black box model, and their interpretability is poor. Numerical simulation methods can simulate complex flow states, and they are widely used in commercial simulators, but at present time-dependent flow conductivity has not been paid much attention.

In response to the above problems, here, we mainly carried out the following two aspects of work: (1) a conductivity test was conducted to study the influence mechanism of different factors on conductivity, and we proposed methods to improve the formula concerning time-dependent conductivity; and (2) based on the EDFM, a shale gas productivity prediction model considering time-dependent conductivity was established, and the model was extended and applied.

## 2. Time-Dependent Effect of Fracture Conductivity

With gas production, the net stress around the fracture increases during the production process; phenomena such as proppant fragmentation, cuttings plugging, and proppant embedding cause the fracture to gradually close; and the fracture conductivity decreases with time. This effect is called time-dependent fracture conductivity [18].

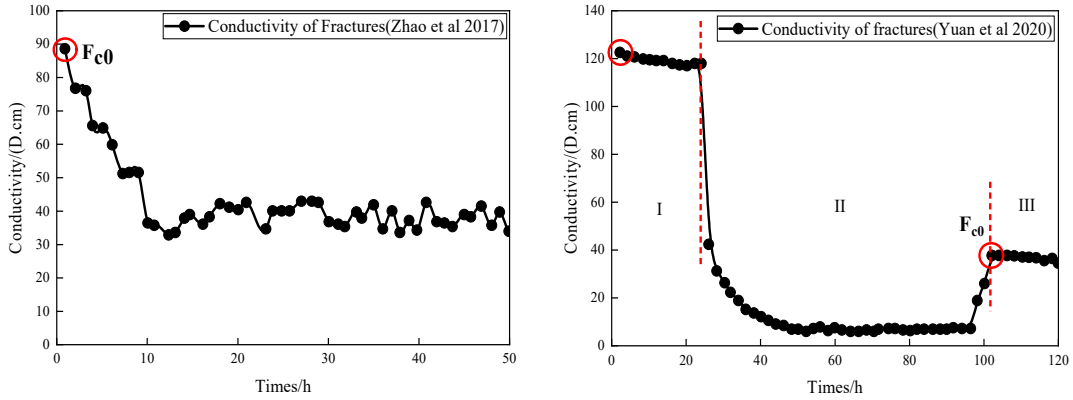
### 2.1. Common Formulas and Problems

There are many factors that affect fracture conductivity, and it is difficult to establish a mathematical model to characterize it through theoretical research. At present, the conductivity function relationship is obtained by fitting the experimental data mainly through laboratory tests. At present, the exponential relationship is commonly used to characterize the change in fracture conductivity with time [19]:

$$F_{ct} = F_{c0}\left(1 + \eta e^{-t/c} - \eta\right) \quad (1)$$

where $F_{ct}$ is the conductivity of the fracture at time $t$; $\eta$ and $c$ is the fitting coefficient; $F_{c0}$ is the conductivity of the fracture at the initial time. However, Equation (1) is inconvenient to use for the following reasons:

(1) An inconsistent experiment process: Figure 1 shows the long-term conductivity test results of shale reservoirs [20,21]. Figure 1a shows the results of a conventional long-term conductivity test in which $F_{c0}$ was equal to the initial conductivity at the start of the test. The gas was injected throughout the test, and the damage to the conductivity caused by the immersion of the fracturing fluid was not considered. In fact, due to the influence of factors such as fracturing and shut-in, the fracture rate of the proppant changes after being soaked in fracturing fluid, and this change affects the change law of conductivity with time.
Figure 1b shows the results of the long-term conductivity test considering the influence of the liquid. The test process was divided into three stages: I. Gas was injected during the test to measure the conductivity at the initial moment; II. Fracturing fluid was injected to simulate the well shut-in, and the process of soaking the proppant in fracturing fluid was carried out; and III. Gas was injected again, and the initial moment of conductivity after the fracturing fluid was soaked was measured and used as $F_{c0}$ in Equation (1). Additionally, we used the process of Figure 1b to conduct experiments in this paper;




(**a**) (**b**)

**Figure 1.** Long-term conductivity test. (**a**) Long-term conductivity test. (**b**) Long-term conductivity test (considering liquids).

(2) Variable experiment parameters: The practicability of Equation (1) is poor. When the test conditions (i.e., field construction parameters) are changed, the test needs to be carried out again to determine the values of $\eta$ and c in Equation (1) under the new test conditions, which undoubtedly increases the time it takes to obtain results.

### *2.2. Long-Term Conductivity Test Experiment*

In view of the above problems, we obtained an improved method for the equation through a long-term conductivity test experiment. The experimental design employed a response surface method. The basic idea behind this methodology is to vary multiple parameters at the same so that maximum inference can be attained with minimum cost, and the method can quantify the relationship between the experimental results and the experimental parameters.

Notably, closure pressure, proppant type, and proppant particle size can be considered constant for a given reservoir condition. Combined with the previous experimental results, we chose the sand concentration, fracturing fluid viscosity, and fracturing fluid residence time as variables. The experimental scheme is shown in Table 1.

**Table 1.** Conductivity Damage Response Surface Factor Level.

| Level | Sand Concentration ($kg/m^2$) | Fluid Viscosity (mPa·s) | Fluid Retention Time (h) |
|---|---|---|---|
| −1 | 5.5 | 1 | 10 |
| 0 | 7 | 3 | 12 |
| 1 | 8.5 | 5 | 14 |

During the experiment, the temperature was kept at a constant of 25°, the closing pressure was 50 MPa, the liquid flow rate was 5 mL/min, and the gas flow rate was 300 mL/min.

In addition, the conductivity retention rate was defined as the ratio of the conductivity before and after fracturing fluid soaking:

$$R_{fg} = \frac{F_{c2}}{F_{c1}} \tag{2}$$

The experimental results are shown in Table 2.

**Table 2.** Results of the response surface test.

| Number | Sand Concentration (kg/m$^2$) | Fluid Viscosity (mPa·s) | Fluid Retention Time (h) | Conductivity Retention Rate (%) |
|---|---|---|---|---|
| 1 | 7 | 3 | 12 | 43.03 |
| 2 | 7 | 3 | 12 | 39.96 |
| 3 | 5.5 | 1 | 12 | 47.61 |
| 4 | 7 | 3 | 12 | 42.38 |
| 5 | 8.5 | 3 | 14 | 47.43 |
| 6 | 7 | 1 | 10 | 56.53 |
| 7 | 7 | 5 | 10 | 32.89 |
| 8 | 7 | 1 | 14 | 51.71 |
| 9 | 8.5 | 1 | 12 | 60.59 |
| 10 | 8.5 | 3 | 10 | 51.08 |
| 11 | 5.5 | 5 | 12 | 26.43 |
| 12 | 7 | 3 | 12 | 41.85 |
| 13 | 5.5 | 3 | 14 | 32.46 |
| 14 | 7 | 3 | 12 | 41.88 |
| 15 | 8.5 | 5 | 12 | 40.34 |
| 16 | 7 | 5 | 14 | 29.11 |
| 17 | 5.5 | 3 | 10 | 36.21 |

The experimental data were processed using Design Expert software, and the regression equation for the prediction of the retention rate of conductivity was obtained:

$$\begin{aligned} R_{fg} &= 41.83 + 7.09A - 10.96B - 2C \\ &+0.2316AB + 0.0238AC + 0.2610BC \\ &+0.5755A^2 + 1.34B^2 - 0.6028C^2 \end{aligned} \tag{3}$$

At the same time, after obtaining $A$ and $B$ in Formula (1) based on the response surface test results, nonlinear polynomial fitting was performed on these values using the test parameters. Finally, the relationship between $A$ and $B$ and sand concentration, fracturing fluid viscosity, and fracturing fluid residence time was obtained:

$$\begin{aligned} \eta &= 5.868 - 0.244A - 0.141B - 0.545C \\ &+0.061AB + 0.028AC - 0.022BC \\ &-0.027A^2 - 0.011B^2 + 0.014C^2 \end{aligned} \tag{4}$$

$$\begin{aligned} c &= 0.036 + 0.021A - 0.003B - 0.014C \\ &+0.0004AB + 0.0002AC - 0.0002BC \\ &-0.002A^2 + 0.0005B^2 + 0.0005C^2 \end{aligned} \tag{5}$$

where $A$ is the sand concentration, $B$ is the fracturing fluid viscosity, and $C$ is the fracturing fluid retention time.

In addition, according to the analysis results of the response surface model, the influences of the three factors on the response value were ranked as fracturing fluid viscosity > sand concentration > fracturing fluid residence time. The coefficient of determination, $R^2$ = 0.9471, of the regression model indicates that the model fit well and the model could be used for prediction.

### *2.3. Amendment to the Formula of Conductivity*

As mentioned above, there are two main aspects to the correction of Equation (1); firstly, the initial conductivity in Equation (1) was corrected using Equation (3) and then using Equations (4) and (5) to modify $\eta$ $c$, and the final formula for the change in conductivity with time can be written as:

$$F_{ct} = F_{c0}R_{fg}(1 + \eta' e^{-t/c'} - \eta') \tag{6}$$

where $R_{fg}$ is the retention rate of conductivity; $\eta'$ $c'$ is the coefficient corrected using Equations (4) and (5).

## 3. Shale Gas Physicomathematical Statements

The high cost of developing unconventional oil and gas resources also means that higher-quality predictive models of production capacity are required to design and manage production processes. The complex migration mechanism of shale gas reservoirs and the development of natural fractures make productivity prediction a challenge.

This section provides a theoretical description of the established shale gas seepage model. Referring to the research results of Wang B et al., the single-phase gas seepage equation in the matrix and fractures can be written as [22]:

$$\frac{\partial}{\partial t}(b\phi_m) + \frac{\partial}{\partial t}\left[\frac{(1-\phi_m)}{\rho_0}q_g\right] = \nabla \cdot \left(\frac{bk_m}{\mu_g}\nabla p_m\right) + bq - bq_{mf} \tag{7}$$

$$\frac{\partial}{\partial t}\left(b\phi_f\right) = \nabla \cdot \left(\frac{bk_f}{\mu_g}\nabla p_f\right) + bq + bq_{mf} \tag{8}$$

where $b$ is the inverse formation volume factor, equal to $\rho_g/\rho_0$; $\rho_g$ is the density of the shale gas in the reservoir, g/cm$^3$; $\phi_m\phi_f$ are the matrix and the fracture porosity, respectively; $q_g$ is the adsorption quality for shale gas, cm$^3$/s; $k_mk_f$ are the corrected matrix and the fracture permeability, respectively, $k = f_1f_2f_3k_0$, D; $\mu_g$ is the viscosity of the shale gas in the reservoir, mPa·s; $q$ is the source and sink, cm$^3$/s; $q_{mf}$ is the leakage term between matrix and fractures, cm$^3$/s.

In addition, to build the model, the following equations are required:

### *3.1. Gas Adsorption*

In terms of organic matter, kerogen, clay minerals in shale, and a large amount of adsorbed gas on the pore surface, there are various isotherm adsorption curves with different forms to describe the isotherm adsorption process of different adsorption systems under different assumptions [23]. The Langmuir isotherm adsorption equation is usually used to describe the adsorption process of shale gas:

$$V = \frac{V_L p}{p_L + p} \tag{9}$$

The mass of gas adsorbed per unit rock volume is:

$$q_g = \frac{V_L p}{p_L + p}\rho_s\rho_{sc} \tag{10}$$

where $\rho_s$ is the density of shale under formation pressure, kg/m$^3$; $V_L$ is the Langmuir volume, m$^3$/kg; $p_L$ is the Langmuir pressure, MPa.

### *3.2. Gas Slip and Spread*

Due to the influence of slippage and diffusion, the flow of shale gas in matrix pores no longer follows Darcy's law. Florence et al. proposed a correction factor for shale gas permeability that can be used to obtain shale gas permeability when slip and Kundsen diffusion are considered [24]:

$$f_1 = (1 + \alpha_k K_n)\left(1 + \frac{4K_n}{1 + K_n}\right) \tag{11}$$

where $\alpha_k$ is the rarefaction coefficient parameter:

$$\alpha_k = \frac{128}{15\pi^2}\tan^{-1}\left(4K_n^{0.4}\right) \tag{12}$$

Additionally, $K_n$ is the Kundsen constant:

$$K_n = \frac{\lambda}{d} \tag{13}$$

### 3.3. Gas Non-Darcy Flow

When the flow velocity in a fracture is too high, there is no longer a linear relationship between the pressure difference and the flow velocity, that is, the high-speed non-Darcy effect occurs. The permeability is corrected using the related concept proposed by Barree et al. [25]:

$$f_2 = \frac{2}{1 + \sqrt{1 + 4\rho\beta\left(\frac{k_0}{\mu}\right)^2 |\nabla p|}} \tag{14}$$

where $\beta$ is the empirical Forchheimer coefficient:

$$\beta = 3.2808 \frac{1.485 \times 10^9}{(k_0 \times 10^{-15})^{1.021}} \tag{15}$$

### 3.4. Time-Dependent Conductivity

In the first section of the paper, the laboratory test of the conductivity test that was carried out is described, and the variation law of the conductivity with time that was obtained is described. Assuming that the fracture width is constant, Equation (6) was used to characterize the change in fracture conductivity:

$$f_3 = R_{fg}(1 + \eta' e^{-t/c'} - \eta') \tag{16}$$

## 4. The EDFM Numerical Model

Lee and Moinfar et al. proposed the embedded discrete fracture model (EDFM), which mathematically treats fractures as well-like sources and "embeds" them into the matrix, avoiding local mesh refinement. Additionally, it can better adapt to the situation of complex fracture distribution [26].

### 4.1. Numerical Discrete

Based on the mathematical model of seepage established above, it is discretized using the finite volume method. The matrix Equation (7) can be written as:

$$\begin{aligned} &\tfrac{\phi_m V_m}{\Delta t}\left(b^{n+1} - b^n\right) + \tfrac{(1-\phi_m) V_m q_g}{\rho_0 \Delta t}\left(p_m^{n+1} - p_m^n\right) \\ &= \nabla\left(V_m \tfrac{k_m}{\mu_g^{n+1}} b^{n+1} \nabla p_m^{n+1}\right) + V_m b^{n+1} q^{n+1} - V_m b^{n+1} q_{mf}^{n+1} \end{aligned} \tag{17}$$

Equation (8) can be written as:

$$\frac{\phi_f V_f}{\Delta t}\left(b^{n+1} - b^n\right) = \nabla\left(V_f \frac{k_f}{\mu_g^{n+1}} b^{n+1} \nabla p_f^{n+1}\right) + V_f b^{n+1} q^{n+1} + V_f b^{n+1} q_{mf}^{n+1} \tag{18}$$

For the meaning of the parameter of Equations (17) and (18), refer to Equations (7) and (8).

### 4.2. Non-Neighbor Connections

For the two-dimensional reservoir model, the fluid in the fracture flowed along the tangential direction of the fracture wall, that is, a one-dimensional flow, and the fracture grid was a line element. Flow exchange occurred between the matrix grid block and the fracture unit in the form of:

4.2.1. Fracture–Matrix NNC

For the fracture–matrix intersection shown in Figure 2 below, the wellhead treatment method in reservoir numerical simulation was used to calculate the channel flow between the fracture and the matrix grid block intersecting with the fracture. Peaceman established a wellhead model for vertical wells, and Lee et al. introduced a well source-like flow coefficient to calculate leakage flow [27]:

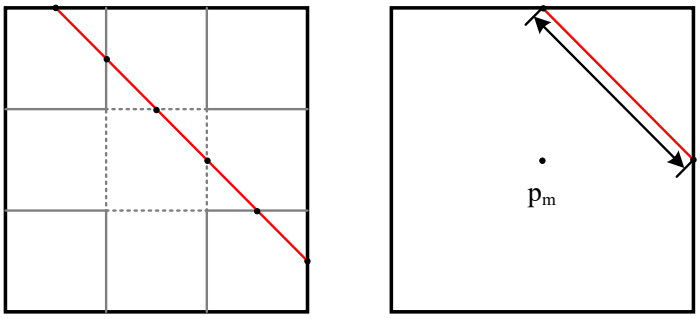



**Figure 2.** Flow exchange between matrix mesh and fracture mesh.

For two-dimensional fluid seepage, the channeling flow between the fracture grid and the matrix grid can be expressed by the following formula:

$$q_{mf} = TI_k\left(p_m^{n+1} - p_f^{n+1}\right) \tag{19}$$

where $TI_k$ is flow coefficient:

$$TI_k = \frac{2k_m l_k h_f}{\mu \overline{d}} \tag{20}$$

where $k_m$ is the matrix permeability, D; $l_k$ is the step size of the crack mesh, m; $h_f$ is the height of fracture, m; $\overline{d}$ is the average distance from the matrix grid block to the fracture, m.

$$\overline{d} = \frac{1}{A}\int l_{xy} dA \tag{21}$$

where $A$ is the area of the matrix grid, $m^2$; $l_{xy}$ is the distance from area element to fracture in matrix mesh, m.

4.2.2. Fracture–Fracture NNC

As shown in Figure 3, multiple fractures intersected for flow exchange, and the volume at the node was much smaller than the grid size of other fractures. If the node also participates in the calculation of the governing equation, the calculation speed will be greatly reduced. Therefore, the conductivity factor between fracture elements was used to determine the flow exchange at the fracture node.

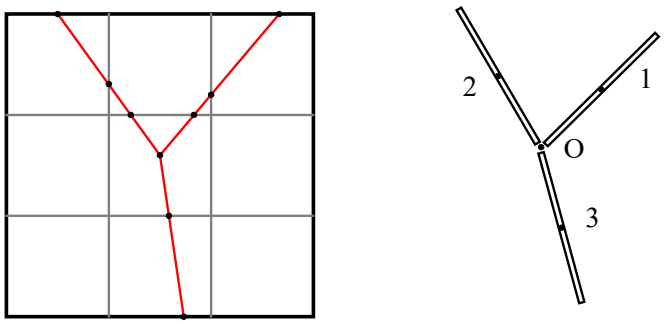



**Figure 3.** Fracture–fracture flow exchange.

When the fracture height was constant, the flow exchange of intersecting fractures at nodes satisfied the material balance equation, namely:

$$\sum_{i=1}^{n} w_{fi} h_f V_{io} = 0 \tag{22}$$

where $w_{fi}$ is the width of fracture, m; $V_{io}$ is the velocity of fracture, m/s.

According to Darcy's law, the flow of fluid flowing into node $O$ through the $i$-th fracture can be obtained:

$$Q_{io} = T_{io}(p_{fo} - p_{fi}) \tag{23}$$

where $T_{io}$ is the conductivity factor:

$$T_{io} = -\frac{2k_{fi} w_{fi} h_f}{\mu l_i} \tag{24}$$

where $k_{fi}$ is the permeability of fracture, D; $l_i$ is the length of fracture grid, m.

Finally, the conductivity factor between the intersecting fractures was determined:

$$T_{ij} = \frac{T_{jo} T_{io}}{\sum_{n=1}^{m} T_{no}} \tag{25}$$

where $T_{ij}$ is the conductivity factor between fractures; $m$ is the total number of intersecting fractures.

#### 4.2.3. Fracture–Well NNC

According to the method proposed by Peaceman et al., the flow conductivity factor between the fracture unit and the well can be expressed as:

$$WI = \frac{2\pi k_f w_f}{\ln(r_e / r_w)} \tag{26}$$

$$r_e = 0.14\sqrt{(\Delta x)^2 + (\Delta y)^2} \tag{27}$$

where $r_e$ is the equivalent well radius, m; $r_w$ is the well radius, m; $\Delta x \Delta y$ are the lengths of the grid in the x and y directions, m, respectively.

### *4.3. Analysis of Model Calculation Results*

#### 4.3.1. Validation

In order to verify the accuracy of the model, the calculation results of the model were compared with the Uncong (Unconventional Oil and Gas Simulator, Ennosoft) commercial simulator. Uncong is a reservoir numerical simulation software. It also uses embedded discrete fractures to simulate fracturing fractures and natural fractures. Physical processes such as Kundsen diffusion and Langmuir adsorption can be considered. The calculation parameters are shown in Table 3.

**Table 3.** Calculated parameters.

| Parameters | Value | Parameters | Value |
|---|---|---|---|
| Model size | 200 × 200m | Fracture permeability | 10,000 mD |
| Number of grids | 100 × 100 | Fracture porosity | 1 |
| Matrix porosity | 0.03 | Fracture length | 100 m |
| Matrix permeability | 0.0001 mD | Fracture width | 0.003 m |
| Langmuir pressure | 9 MPa | Initial formation pressure | 30 MPa |
| Langmuir volume | 0.004 $m^3$/kg | Bottom hole pressure | 15 MPa |

Figure 4 shows the cumulative production calculation for one year of production with the model set to constant conductivity. The error between the model production calculation results and the Uncong calculation results was 3.11%. In the early stage, the model calculation results showed good consistency with the Uncong calculation. As production progressed, the model calculations were slightly lower than the Uncong calculation. Errors may have occurred due to differences in solution methods and in differences in some mechanism models.

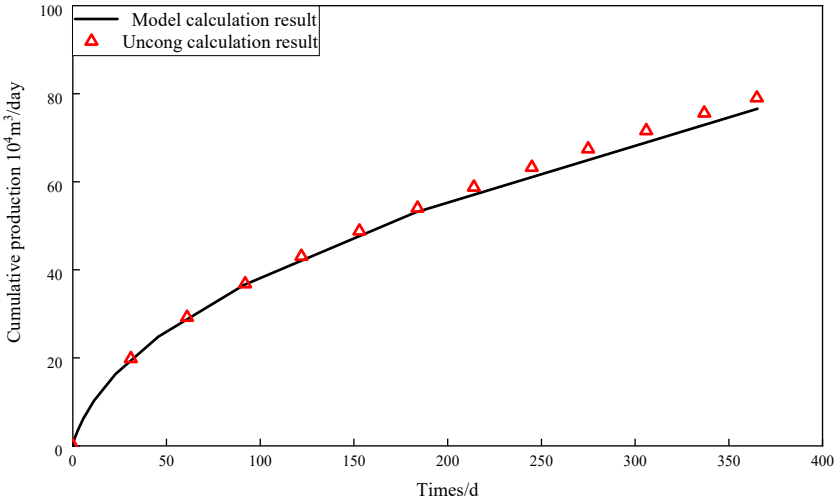
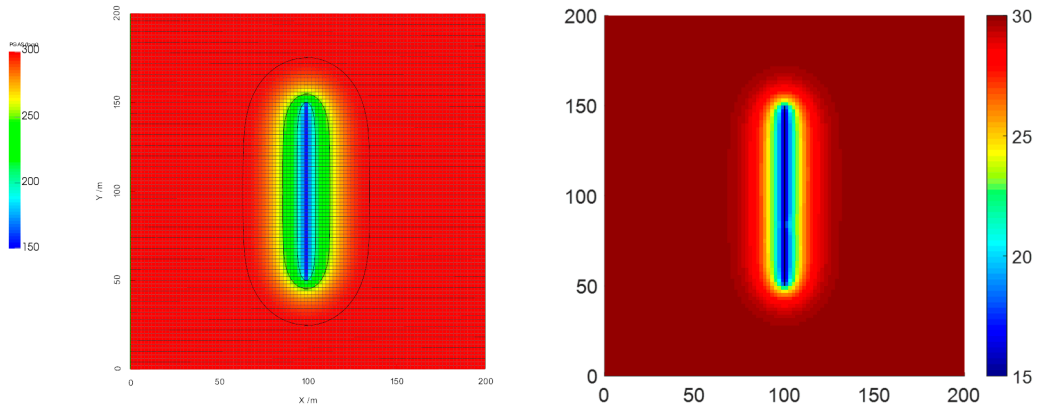



**Figure 4.** Cumulative production (model vs. Uncong).

In addition, in order to facilitate the comparison of formation pressure changes (Figure 5), the authors set formation pressure contours in the Uncong calculation results. It can be seen from the settlement results that the two maintained good consistency.




(**a**) (**b**)

**Figure 5.** Formation pressure (model vs. Uncong). (**a**) Result from Uncong. (**b**) Result from model.

#### 4.3.2. Analysis of Flow and Pressure Changes in Fractures

The formation pressure was set to 30 MPa, the bottom hole pressure was 15 MPa, the initial fracture permeability was 10D, $\eta$ = 0.9, $c$ = 0.008, the model size was 300 × 300, the number of matrix grids was 100 × 100, and the production time was 1 year. The variation law of fracture flow and the pressure in different production times were studied under constant conductivity and variable conductivity conditions. Figure 6 shows the formation pressure changes corresponding to different production times.

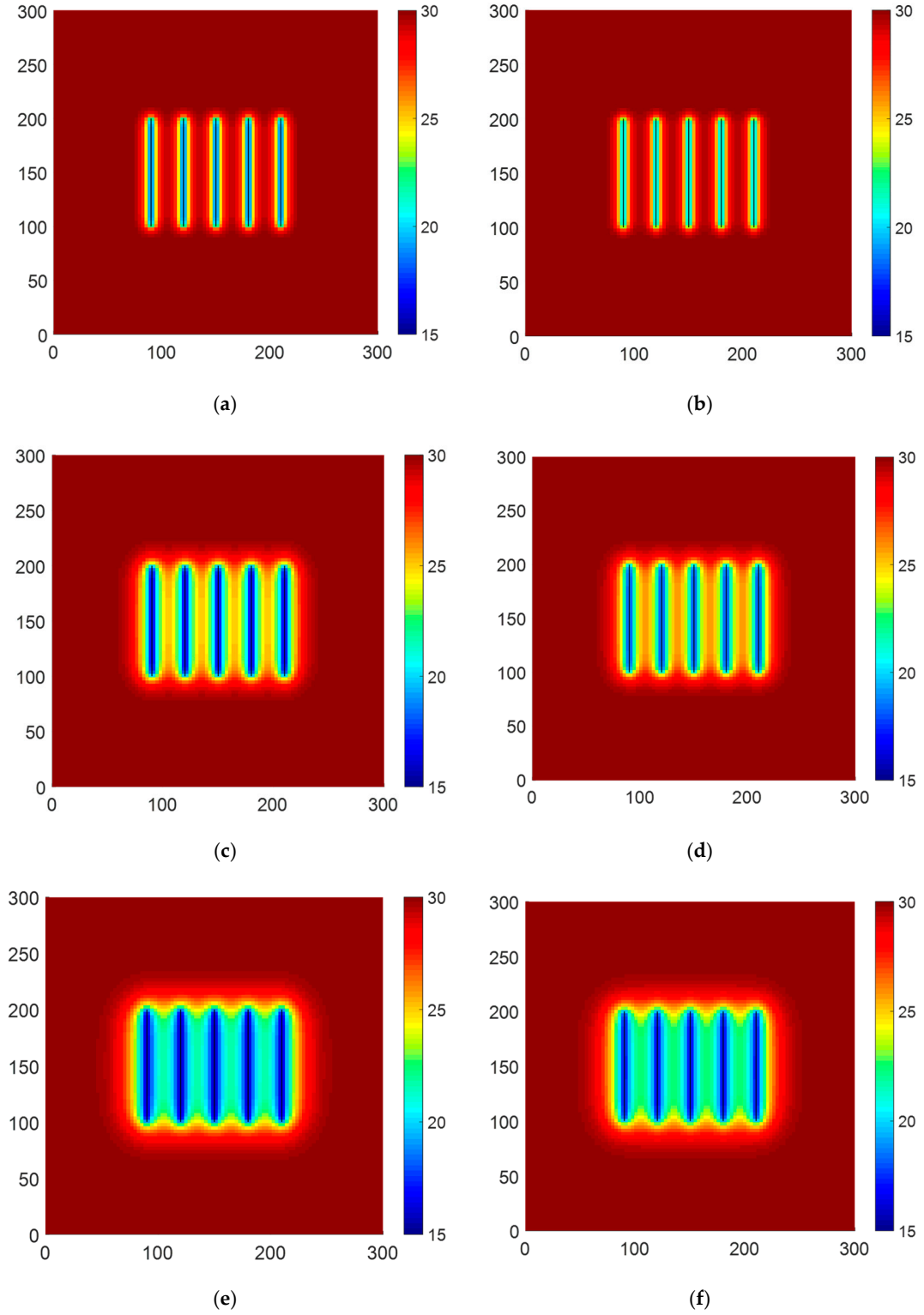



**Figure 6.** Formation pressure at different production times. (**a**) Pressure of production, 50d (constant conductivity). (**b**) Pressure of production, 50d (variable conductivity). (**c**) Pressure of production, 180d (constant conductivity). (**d**) Pressure of production, 180d (variable conductivity). (**e**) Pressure of production, 1y (constant conductivity). (**f**) Pressure of production, 1y (variable conductivity).

Figure 7 shows the pressure distribution at the near-wellbore location corresponding to different times. In both cases, the pressure near the wellbore exhibited a distinct "funnel" shape. In the early stage of production (50d), the "funnel" curves of the two cases almost

overlapped, but the "funnel" that corresponded to the constant conductivity pressure curve was deeper, indicating that the flow into the wellbore was larger under the constant conductivity, so the drop in pressure was larger [28].

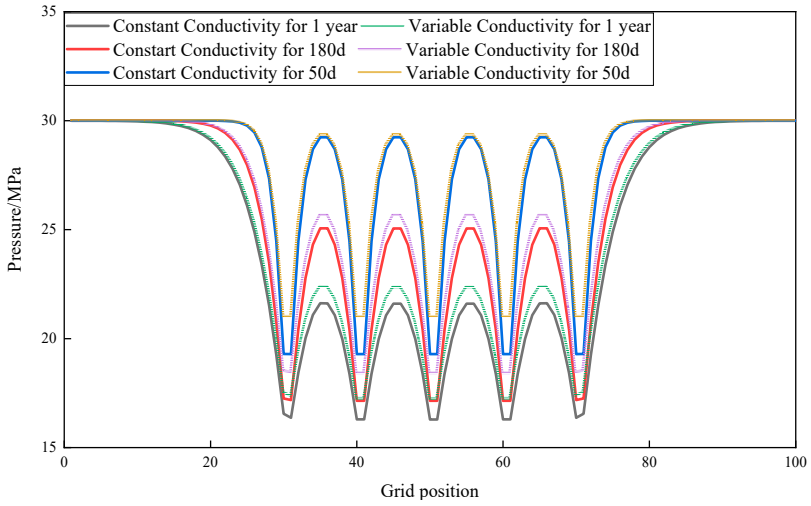



**Figure 7.** Pressure distribution near wellbore.

With the progress of production, the "funnel" of the variable conductivity pressure curve gradually separated from the "funnel" of the constant conductivity pressure curve. This is because the fracture conductivity gradually decreased under the condition of variable conductivity, and less fluid flowed into the fracture. The pressure around the fracture was higher, so the "funnel" of the variable conductivity pressure curve was thinner than the "funnel" of the constant conductivity pressure curve.

Figure 8 displays the flow distribution curve of the well point location. In the early stage of production, the flow rates at each well point in the two cases were quite different, and both appeared as a straight line. With the increase in time, the inter-fracture interference became stronger, and the fractures at both ends were less disturbed and had a larger oil drainage area. This meant that the production rate was higher, displaying an upward trend at both ends.

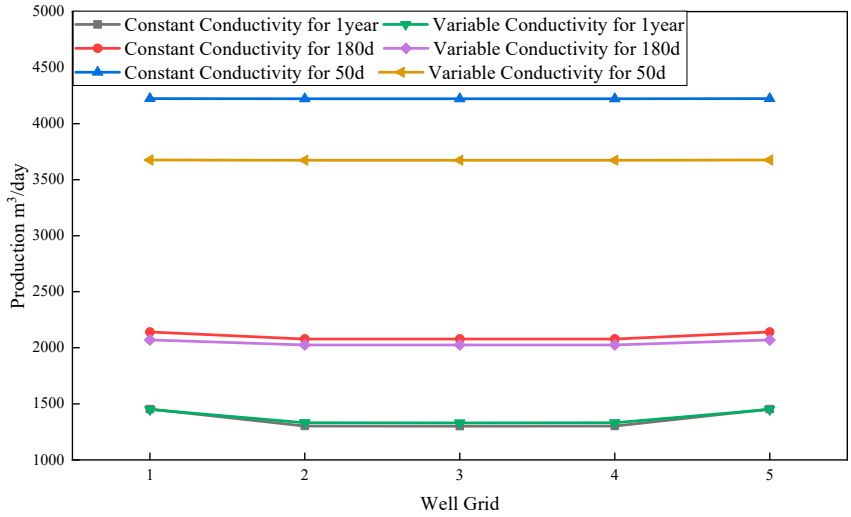



**Figure 8.** Near well flow distribution.

In addition, the connecting line of the middle well point was approximately a straight line in both cases, but the upturn of both ends of the flow curve of variable conductance was not obvious. This also means that, in actual production, if the change in conductivity

over time is considered, the production of the fractures at both ends may be lower than the value expected by reservoir engineers.

#### 4.3.3. Effects of Complex Fractures

Several branch fractures were added around the artificial fractures to simulate production under complex fracture morphology. The parameter settings were consistent with the previous section, the production time was one year, and the calculation results regarding pressure and cumulative output are shown in the figure below.

Figure 9 shows the cloud map of formation pressure under the conditions of constant conductivity and variable conductivity for one year. It can be seen from the figure that the range and the degree of the formation pressure drop was smaller when the production with variable conductivity was used. This is because the initial production of shale reservoirs mainly comes from artificial fractures. As the production progressed, the proppant was embedded and broken, resulting in the gradual closure of artificial fractures, and the decrease in conductivity led to an increase in the flow resistance of fluids, so the formation pressure dropped more slowly [29].

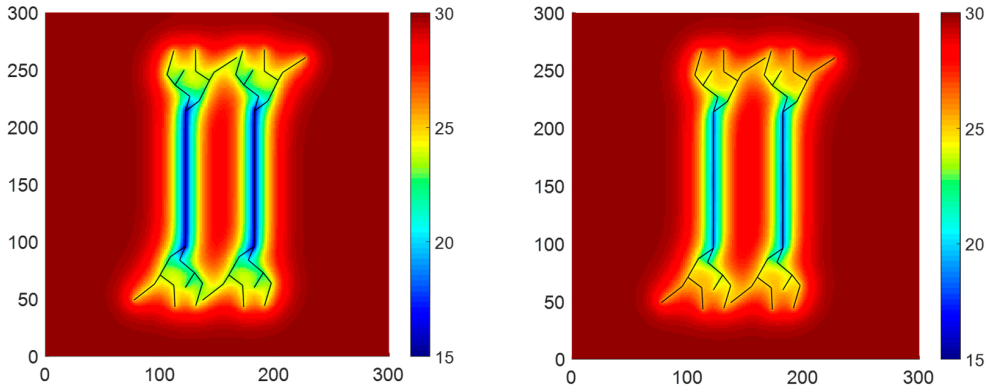



**Figure 9.** Formation pressure (constant conductivity vs. variable conductivity).

Figure 10 shows a comparison of one year of cumulative production under constant and variable conductivity conditions. It can be seen from the figure that the cumulative output that corresponded to the variable conductivity was smaller than the cumulative output that corresponded to the constant conductivity, and the final output differed by 19%, indicating that the time-varying effect of conductivity on the actual output cannot be ignored.

#### 4.3.4. Effects of Natural Fractures

In order to consider the production situation under the condition of natural fractures, 50 natural fractures were randomly distributed in the reservoir, and the rest of the calculation parameters and grid division were consistent with the previous section.

Figure 11 displays the cloud map of formation pressure under the condition of natural fractures. Compared with the situation that did not consider natural fractures, natural fractures were shown to strengthen the connection between artificial fractures and the reservoir, which was equivalent to increasing the matrix permeability to a certain extent, so the pressure wave propagated faster in the reservoir and the drop in pressure was more obvious.

On the other hand, although the presence of natural fractures resulted in a faster drop in pressure, there was still a significant difference in the formation pressure distribution between the two cases (constant versus variable conductivity). This is consistent with the conclusion obtained above: as production progresses, the conductivity gradually decreases. The greater the decline rate or the faster the decline rate, the shorter the stable production period of the gas well and the earlier the decline in production.

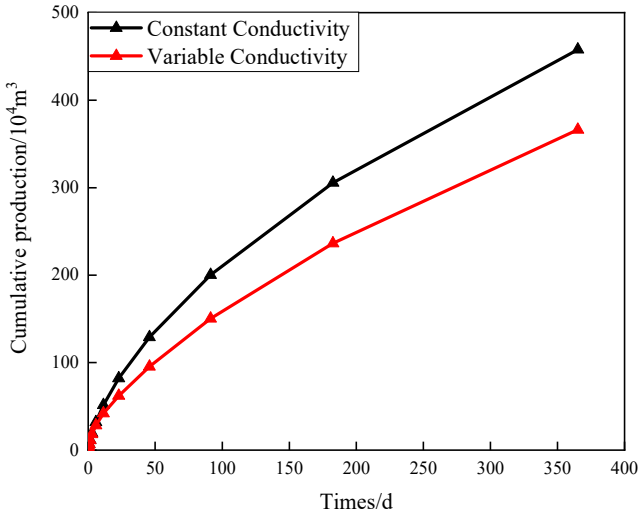



**Figure 10.** Cumulative production (constant conductivity vs. variable conductivity).

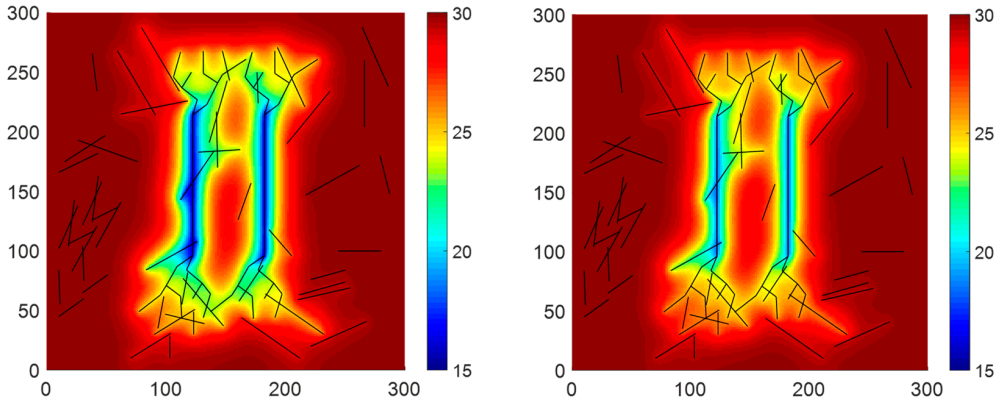



**Figure 11.** Formation pressure (constant conductivity vs. variable conductivity).

Figure 12 shows the comparison of one year of cumulative production under the conditions of constant conductivity and variable conductivity. Compared with the previous section, the existence of natural fractures increased the production in both cases (constant conductivity vs. variable conductivity) by 14% and 13%, respectively. The cumulative yield that corresponded to constant conductivity and the cumulative yield that corresponded to variable conductivity differed by 21%.

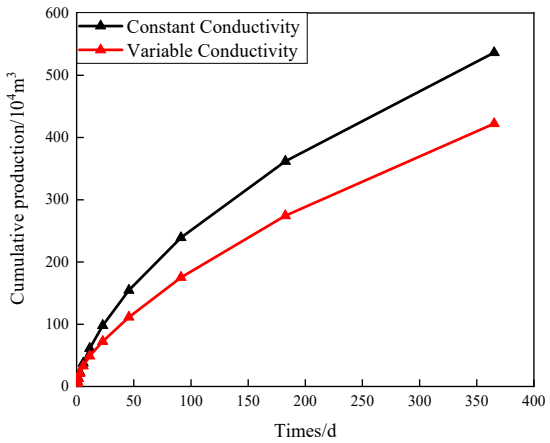



**Figure 12.** Cumulative production (constant conductivity vs. variable conductivity).

## 5. Application Case

Using data from Well W1 in the China Shale Gas Field to verify the productivity prediction model, the depth of the well was 2531 m, the formation pressure was 35 MPa, the permeability was 2.08 × $10^{-4}$ mD, the porosity was 5%, the compressibility was 1.05 × $10^{-4}$ $MPa^{-1}$, the fracture length was 120 m, the height was 40 m, and the width was 0.003 m. The fracturing parameters of this well were used in Equations (4)–(6) to calculate $R_{fg}$ = 72.01%, $\eta$ = 0.4, $c$ = 0.003. The production performance of the well was evaluated using the established productivity prediction model, considering the effect of variable conductivity. The comparison results are shown in Figure 13.

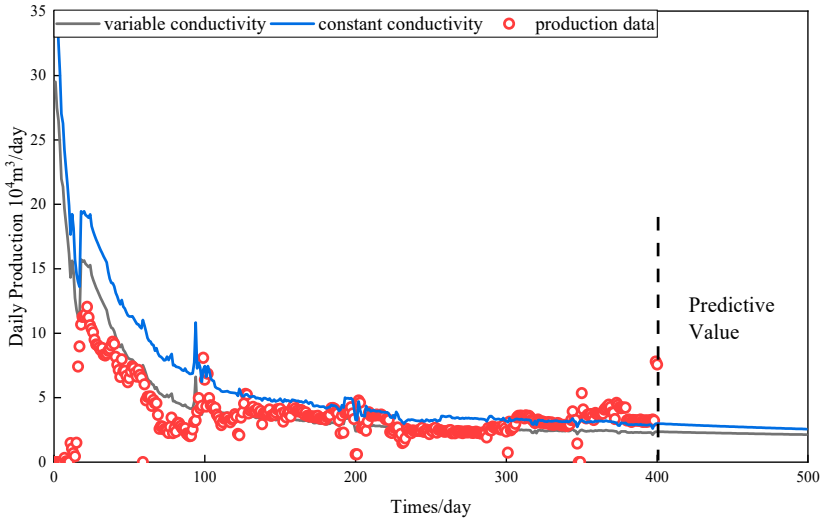



**Figure 13.** Comparison between actual production data and model prediction data of Well W1.

In the early stage of production, the decline in conductivity was the largest, so compared with the calculation results of the constant conductivity model, the calculation results of the variable conductivity model were most similar to the actual production data in the early stage. Although the conductivity decreased in the later stage of production, the magnitude was small, so the difference between the calculation results of the constant conductivity model and the variable conductivity model in the later stage of production was small.

Generally speaking, the error between the calculation result of the variable conductivity model and the actual situation was 18%, which means the variable conductivity model was more consistent with the actual situation, and the production capacity forecast needs to consider the change in conductivity over time.

## 6. Conclusions

(1) The order of significance of the test factors on the conductivity retention rate is: fracturing fluid viscosity > sand concentration > fracturing fluid retention time.

(2) According to the experimental data, the relationship between $R_{fg}$, $\eta$, and $c$ and the fracturing fluid viscosity, sand concentration, and fracturing fluid residence time was fitted. An improved method for the formula of the dependent conductivity was proposed, and this formula is more practical.

(3) A prediction model of shale gas production was established, and its accuracy was verified using the commercial simulator Uncong (the error of the calculation result was 3.11%). The analysis results of the flow change law in the fracture show that, compared with the constant conductivity flow curve, the upturn at both ends of the variable conductivity flow curve was not obvious; the analysis results of the pressure change law in the fracture show that the "funnel" of the pressure curve of variable conductivity under the same time was thinner and shorter.

(4) We investigated the impact on production performance in the presence of complex fractures and in the presence of natural fractures. In both cases, the cumulative production of the constant conductivity model and the variable conductivity model could be increased, but the cumulative production increase corresponding to the variable conductivity model was smaller than that of the constant conductivity model.

(5) The practical application results show that the production prediction model considering the time-dependent conductivity was closer to the production data, with an error of 18%. This shows that time-dependent conductivity cannot be ignored in the production forecast.

**Author Contributions:** Conceptualization, Y.P.; methodology, Y.P.; software, Y.P.; validation, Y.P.; formal analysis, Y.P.; investigation, Y.X.; resources, Y.X.; data curation, Z.Y.; writing—original draft preparation, Y.P.; writing—review and editing, C.W.; visualization, Z.Y.; supervision, R.L.; project administration, R.L.; funding acquisition, R.L. All authors have read and agreed to the published version of the manuscript.

**Funding:** This research was funded by [National Natural Science Foundation of China] grant number [62173049].

**Conflicts of Interest:** The authors declare no conflict of interest.

## References

1. Kuuskraa, V.A. Unconventional natural gas, industry savior or bridge? In Proceedings of the EIA Energy Outlook and Modeling Conference, Washington, DC, USA, 27 March 2006.
2. Li, X.; Hu, S.; Cheng, K. Suggestions from the development of fractured shale gas in North America. *Pet. Explor. Addit. Dev.* **2007**, *34*, 392–400.
3. Zhang, J.; Jin, Z.; Yuan, M. Reservoiring Mechanism of Shale Gas Additionally, Its Distribution. *Nat. Gas Ind.* **2004**, *24*, 15–18.
4. Zhang, L.; Xu, B.; Xin, C.; Qiao, X.; Mu, J.; Xu, Y.; Han, C. Production forecasting model of shale gas considering the main fractures. *Nat. Gas Geosci.* **2019**, *30*, 247–256. [CrossRef]
5. Li, Y.; Liu, X.; Hu, Z.; Duan, X.; Zhang, J.; Zhan, H. Summary of numerical models for predicting productivity of shale gas horizontal wells. *Adv. Earth Sci.* **2020**, *35*, 350–362.
6. Kelvin, A.; John, W.; Derek, E. Laboratory Investigation of Impact of Slickwater Composition on Multiphase Permeability Evolution in Tight Sandstones. *SPE Prod. Oper.* **2021**. [CrossRef]
7. Antonia, S.; Victor, T.; Ulrich, B. Assessment of Polymer-Induced Clogging Using Microfluidics. *SPE J.* **2021**, *26*, 3793–3804.
8. Jesse, G.; Zhu, D.; Hill, A.D. Impairment of Fracture Conductivity in the Eagle Ford Shale Formation. *SPE Prod. Oper.* **2018**, *33*, 637–653.
9. Jansen, T.; Zhu, A.D. The Effect of Rock Mechanical Properties on Fracture Conductivity for Shale Formations. In Proceedings of the SPE Hydraulic Fracturing Technology Conference, The Woodlands, TX, USA, 3–5 February 2015.
10. Abhinav, M.; Chandra, S.; Carl, H. A Study of Propped-Fracture Conductivity: Impairment Mechanisms Under Laboratory Conditions. In Proceedings of the SPWLA 58th Annual Logging Symposium, Oklahoma City, OK, USA, 17–21 June 2017.
11. Zhang, J.J.; Ouyang, L.; Hill, A.D. Experimental and Numerical Studies of Reduced Fracture Conductivity due to Proppant Embedment in Shale Reservoirs. In Proceedings of the SPE Annual Technical Conference and Exhibition, Amsterdam, The Netherlands, 27–29 October 2014.
12. Awoleke, O.O.; Zhu, D. New propped-fracture-conductivity models for tight gas sands. *SPE J.* **2016**, *21*, 1508–1517. [CrossRef]
13. Yu, J.; Wang, J.; Wang, S. Propped Fracture conductivity Evolution during Reservoir Drawdown. In Proceedings of the 55th U.S. Rock Mechanics/Geomechanics Symposium, Houston, TX, USA, 18–25 June 2021.
14. Wang, J.; Elsworth, D.; Denison, M.K. Proppant transport in a propagating hydraulic fracture and the evolution of transport properties. In Proceedings of the 53rd U.S. Rock Mechanics/Geomechanics Symposium, New York, NY, USA, 23–26 June 2019.
15. Guo, X.; Zhou, C. Diffusion Seepage Model for Fractured Horizontal Well in Shale Gas Reservoir. *J. Southwest Pet. Univ.* **2015**, *37*, 38–44.
16. Wei, Y.; Wang, J.; Yu, W.; Qi, Y.; Miao, J.; Yuan, H.; Liu, C. A smart productivity evaluation method for shale gas wells based on 3D fracture network model. *Pet. Explor. Dev.* **2021**, *48*, 787–796. [CrossRef]
17. Pan, Y.; Wang, Y.; Che, M.; Liao, R.; Zheng, H. Post-fracturing production prediction and fracturing parameter optimization of horizontal wells based on grey relation projection random forest algorithm. *J. Xi'Shiyou Univ.* **2021**, *36*, 71–76. [CrossRef]
18. Wang, X.; Feng, D.; Li, X.; Yan, Y.; Guo, X.; Qiao, X.; Xue, B.; Ma, C.; Wang, Q.; Lei, K.; et al. Productivity evalution of tight gas well with time-dependent mechanism: A case study of Yan'an gasfield. *Acta Pet. Sin.* **2019**, *40*, 1358–1367.
19. Wen, Q.; Zhang, S.; Wang, L.; Liu, Y.; Li, X. The effect of proppant embedment upon the long-term conductivity of fractures. *J. Pet. Sci. Eng.* **2007**, *55*, 221–227. [CrossRef]
20. Zhao, Y.; Zhang, S.; Xiao, F.; He, J.; Dong, Y.; Zhao, W. Experimental study on long-term flow conductivity of fractured fractures in different types of reservoirs. *Sci. Technol. Eng.* **2017**, *17*, 192–197.

21. Yuan, X.; Xu, D.; Chen, S.; He, X.; Cheng, N.; Chen, J. The damage of fracturing fluid intrusion to the conductivity of shale reservoir. *Sci. Technol. Eng.* **2020**, *20*, 3591–3597.
22. Wang, B.; Fidelibus, C. An Open-Source Code for Fluid Flow Simulations in Unconventional Fractured Reservoirs. *Geosciences* **2021**, *11*, 106. [CrossRef]
23. Gregg, S.J.; Sing, K.S. *Adpsorption, Surface Area and Porosity*; Academic Press: London, UK, 1982.
24. Beskok, A.; Karniadakis, G.E. Report: A model for flows in channels, pipes, and ducts at micro and nanoscales. *Microscale Thermophys. Eng.* **1999**, *3*, 43–77.
25. Barree, R.D.; Conway, M.W. Beyond beta factors: A complete model for Darcy, Forchheimer, and trans-Forchheimer flow in porous media. In Proceedings of the SPE Annual Techical Conference and Exhibition, Houston, TX, USA, 26–29 September 2004.
26. Lee, S.H.; Lough, M.F.; Jensen, C.L. Hierarchical modeling of flow in naturally fractured formations with multiple length scales. *Water Resour. Res.* **2001**, *37*, 443–455. [CrossRef]
27. Peaceman, D.W. Interpretation of well-block pressures in numerical reservoir simulation. *SPE J.* **1978**, *19*, 183–194.
28. Li, Z.; Wu, X.; Han, G.; Wang, R.; Zheng, L. Semi-analytical model of multi-stage fractured horizontal well productivity considering time-dependent fracture conductivity. *Oil Drill. Prod. Technol.* **2019**, *41*, 354–362.
29. Chen, X. Fracturing Fluid Flowback Simulation of Fractured Horizontal Well in Shale Gas Reservoirs. Doctoral Dissertation, Southwest Petroleum University, Chengdu, China, 2019.